Ferrous Ion Binding to Recombinant Human H-Chain Ferritin. An Isothermal Titration Calorimetry Study†

Fadi Bou-Abdallah,‡ Paolo Arosio,§ Paolo Santambrogio,‖ Xiaoke Yang,‡ Christine Janus-Chandler,‡ and N. Dennis Chasteen*,‡

Department of Chemistry, University of New Hampshire, Durham, New Hampshire 03824, Chemistry Section, Faculty of Science, University of Brescia, 25123 Brescia, Italy, and Protein Engineering Unit, IRCCS H. San Raffaele, Via Olgettina 58, 20132 Milano, Italy

Received March 18, 2002; Revised Manuscript Received July 8, 2002

ABSTRACT: Iron deposition within the iron storage protein ferritin involves a complex series of events consisting of Fe^{2+} binding, transport, and oxidation at ferroxidase sites and mineralization of a hydrous ferric oxide core, the storage form of iron. In the present study, we have examined the thermodynamic properties of Fe^{2+} binding to recombinant human H-chain apoferritin (HuHF) by isothermal titration calorimetry (ITC) in order to determine the location of the primary ferrous ion binding sites on the protein and the principal pathways by which the Fe^{2+} travels to the dinuclear ferroxidase center prior to its oxidation to Fe^{3+}. Calorimetric titrations show that the ferroxidase center is the principal locus for Fe^{2+} binding with weaker binding sites elsewhere on the protein and that one site of the ferroxidase center, likely the His65 containing A-site, preferentially binds Fe^{2+}. That only one site of the ferroxidase center is occupied by Fe^{2+} implies that Fe^{2+} oxidation to form diFe(III) species might occur in a stepwise fashion. In dilute anaerobic protein solution (3−5 μM), only 12 Fe^{2+}/protein bind at pH 6.51 increasing to 24 Fe^{2+}/protein at pH 7.04 and 7.5. Mutation of ferroxidase center residues (E62K+H65G) eliminates the binding of Fe^{2+} to the center, a result confirming the importance of one or both Glu62 and His65 residues in Fe^{2+} binding. The total Fe^{2+} binding capacity of the protein is reduced in the 3-fold hydrophilic channel variant S14 (D131I+E134F), indicating that the primary avenue by which Fe^{2+} gains access to the interior of ferritin is through these eight channels. The binding stoichiometry of the channel variant is one-third that of the recombinant wild-type H-chain ferritin whereas the enthalpy and association constant for Fe^{2+} binding are similar for the two with an average values ($\Delta H° = 7.82$ kJ/mol, binding constant $K = 1.48 \times 10^5$ M^{-1} at pH 7.04). Since channel mutations do not completely prevent Fe^{2+} binding to the ferroxidase center, iron gains access to the center in approximately one-third of the channel variant molecules by other pathways.

Iron is an important element for the growth and development of most organisms but is also potentially toxic and exhibits poor bioavailability. Hence, the ability to store and release iron in a controlled fashion is essential for homeostasis. Cells solve this problem by using ferritins, a family of iron-storage proteins that sequester iron as a hydrous ferric oxide mineral similar in structure to the mineral ferrihydrite ($Fe_2O_3 \cdot nH_2O$). Mammalian ferritins are composed of 24 subunits of two types, H and L (*1*) assembled to form a hollow spherical structure with inner and outer diameters of approximately 80 and 120 Å, conveniently described as a truncated rhombic dodecahedron of 4:3:2 symmetry (*2*−*4*). Each ferritin subunit is a bundle of four (A, B, C, D) α-helices with a short fifth (E) α-helix at the C-terminus and a loop connecting the antiparallel helix pairs A−B and C−D. The H- and L-subunits have complementary roles in iron oxidation and mineralization (*5*). The H-subunit contains a dinuclear ferroxidase center (Figure 1) at which Fe^{2+} oxidation by O_2 is rapidly catalyzed (*6*, *7*), whereas the L-subunit lacks such a center and appears to provide nucleation sites for mineralization at glutamate and aspartate residues located on the inner surface of the protein shell (*8*).

The formation of the iron mineral core is a multistep, protein-mediated process which involves the binding of Fe^{2+} to protein sites, the oxidation of bound Fe^{2+} to Fe^{3+} by molecular oxygen, the hydrolysis of the resulting Fe^{3+}, and finally the nucleation of a ferrihydrite-like mineral within the ferritin cavity. The mechanism of iron sequestration within the protein shell and the pathways by which Fe^{2+} travels to the ferroxidase center prior to its oxidation to Fe^{3+} have been subjects of intense investigation (*3*, *15*−*20*). During iron core formation, Fe^{2+} is thought to enter the protein through one or more channels (*9*, *10*). Possible pathways include the eight hydrophilic channels on the 3-fold axes (*10*−*13*), the 2-fold axes (*4*) and the 1-fold channel on the H-subunit (*2*). The hydrophilic character of the 3-fold

† This work was supported by Grant R37 GM20194 from the National Institute of General Medical Sciences (N.D.C.), by the Italian Ministry of the University and Research (MURST) Cofin-2000−01 (P.A.), and by CNR Agenzia 2000 (P.A.).

* To whom correspondence should be addressed. Department of Chemistry, Parsons Hall, University of New Hampshire, Durham, NH 03824. Phone: (603) 862-2520. Fax (603) 862-4278. E-mail: ndc@cisunix.unh.edu

‡ University of New Hampshire.

§ University of Brescia.

‖ IRCCS H. San Raffaele.

10.1021/bi020215g CCC: $22.00 © 2002 American Chemical Society
Published on Web 08/23/2002

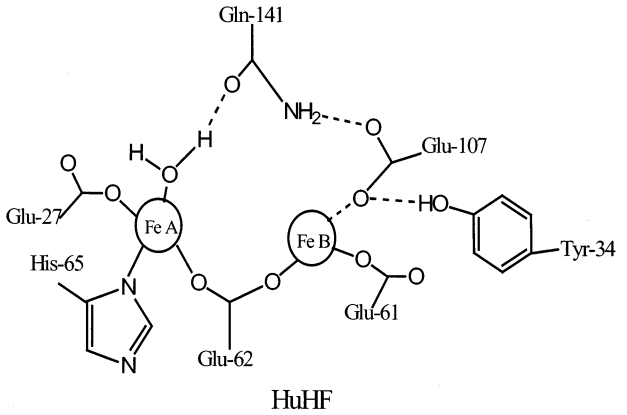

FIGURE 1: Schematic diagram of the dinuclear ferroxidase sites of human H-chain ferritin (HuHF) in the diferrous form based on the crystal structure of the Tb^{3+} derivative (*2*, *3*). The drawing was made with ChemDraw structure drawing program manufactured by CambridgeSoft.

channels makes them one of the most reasonable routes for iron entry into ferritin consistent with initial binding of Fe^{2+} presumably occurring at residues located along the 3-fold axes (*10*, *13*, *14*).

A study of Fe^{2+} binding to horse spleen ferritin (HoSF) under anaerobic conditions employing size-exclusion chromatography and Mössbauer spectroscopy has revealed that approximately 8.0 Fe^{2+} bind per protein molecule, suggesting binding within the eight hydrophilic channels (*21*). However, direct information about the binding sites for Fe^{2+} has been lacking. The number and location of the primary binding sites on the protein and their affinity for Fe^{2+} have not been defined nor have the thermodynamic parameters for Fe^{2+} binding, oxidation, and Fe^{3+} mineralization been previously measured.

In the present paper, we use isothermal titration calorimetry (ITC) to investigate Fe^{2+} binding to HuHF[1] and to three H-chain site-directed variants: ferroxidase center variant 222, in which the two ligands Glu62 and His65 of the ferroxidase center are changed (E62K + H65G); 3-fold channel variant S14 in which the 3-fold channel site ligands Asp131 and Glu134 are changed (D131I + E134F); and variant A2 in which the nucleation site ligands Glu61, Glu64, and Glu67 are changed (E61A + E64A + E67A). The results of this study show that, in the absence of oxygen and at pH 7.0–7.5 in dilute conditions, 24 Fe^{2+} bind to each HuHF molecule, one per each of the 24 ferroxidase centers of the protein. A difference in the affinity of Fe^{2+} for the two sites of the dinuclear ferroxidase center is demonstrated. Mutation of the ferroxidase site ligands Glu62 and His65 totally eliminates the strong binding of Fe^{2+} to the ferroxidase site whereas mutation of the nucleation site ligands has little effect on Fe^{2+} binding. The 3-fold channels are shown to be important pathways for Fe^{2+} entry into the interior of the protein shell; mutation of the Asp and Glu residues of the 3-fold channels reduces the amount of Fe^{2+} that gains access to the ferroxidase centers. At high Fe^{2+} and protein concentrations, additional weak binding sites of unknown origin are observed.

MATERIALS AND METHODS

Reagent grade chemicals were used directly; ferrous sulfate heptahydrate, $FeSO_4 \cdot 7H_2O$ (J. T. Baker Chemical Co.), Mes and Mops (Research Organics), 2,2′-dipyridyl and sodium chloride (Aldrich Chemical Co.), and β-D(+)-glucose (Sigma Chemical Co.). Beef liver catalase (EC 1.11.1.6), 65000 U/mg and *Aspergillus niger* glucose oxidase (GOD) grade I, 25000 U/84.5 mg, were purchased from Boehringer-Mannheim GmbH (Germany). Recombinant H-chain ferritin and H-chain variants were prepared as previously described (*22*, *23*) and rendered iron free by dialysis against sodium hydrosulfite (dithionite), $Na_2S_2O_4$, and complexation with 2,2′-bipyridyl at pH 6.0 (*24*). Protein concentrations were determined using the Advanced Protein Assay (http://Cytoskeleton.com, patent pending), or spectrophotometrically using the molar absorptivity of 23 000 cm^{-1} M^{-1} at 280 nm for the apoprotein (*25*).

Isothermal titration calorimetry (ITC) measurements were carried out at 25.00 °C on a CSC Model 4200 isothermal titration calorimeter (Calorimetry Science Corporation). The fundamental principles of isothermal titration calorimetry are described elsewhere (*26*). Titrant and sample solutions were made from the same stock buffer solution and thoroughly deoxygenated before each titration using an aspirator and high purity argon gas (99.995%, <5 ppm O_2). All the experiments involving the air-sensitive Fe^{2+} state of ferritin were conducted under anaerobic conditions with an atmosphere of argon. In these anaerobic experiments, either dithionite ($Na_2S_2O_4$) or glucose/glucose oxidase (GOD) plus catalase was added to the protein solution to prevent Fe^{2+} oxidation from possible residual O_2. Identical results were obtained using either method of excluding O_2. The protein solution was stirred at 297 rpm to ensure rapid mixing of the titrant upon injection. The instrument was calibrated by means of a known standard electrical pulse (20 pulses of 200 μJ each with 200 s interval between pulses) and by a chemical calibration (Ba^{2+} binding to 18-crown-6) (*27*). All aspects of the instrument (calibration constant, cell volume and injection volume) were tested. Typically, an automated sequence of 25 injections, each of 10 μL titrant into the sample cell, spaced at 5 min intervals to allow complete equilibration, were performed with the equivalence point coming at the area midpoint of the titration. The area under the resulting peak following each injection, is proportional to the heat of interaction Q, which is normalized by the concentration of the added titrant and corrected for the dilution heat to give the molar binding enthalpy $\Delta H°$. All experiments were repeated two to four times with a background correction using the buffer solution alone to account for the heat of dilution. It was noted that increasingly larger exothermic heats of dilution were obtained as the 10 μL aliquots of ~1.5 mM Fe(II) solution was repeatedly titrated into 1.3 mL cell containing buffer alone at pH 7.0 and 7.5 with heats of dilution ranging from −30 to −150 μJ for the first to the 25th addition. The lower value for the heat of dilution was chosen for correcting all data. The choice of heat of dilution does not appreciably affect the binding

[1] Abbreviations: HuHF, recombinant human H-chain wild-type ferritin; HoSF, horse spleen ferritin; BfMF, bullfrog M-chain ferritin; EcFtnA, *Escherichia coli* bacterial ferritin; ITC, isothermal titration calorimetry; DSC, differential scanning calorimetry; Mes, 2-(*N*-morpholino) ethanesulfonic acid; Mops, 3-(*N*-morpholino) propanesulfonic acid; A2, nucleation site variant (E61A + E64A + E67A); S14, 3-fold channel variant (D131I + E134F); 222, ferroxidase center variant (E62K + H65G and also K86Q).

Table 1: Best Fit Parameters for ITC Measurements of Fe^{2+} Binding to HuHF and Its variants at 25.00 °C[a]

protein in buffer	n_1	K_1 (M^{-1})	ΔH_1^0 (kJ/mol)	ΔG_1^0 [b] (kJ/mol)	ΔS_1^0 [c] (J/mol·K)
HuHF in 50 mM Mes, 100 mM NaCl, pH 6.51 (Figure 2)	11.47 ± 0.47	(1.22 ± 0.24) × 10^5	8.94 ± 0.30	−29.03 ± 0.62	127.35 ± 0.64
HuHF in 50 mM Mops, 100 mM NaCl, pH 7.04 (Figure 3)	25.03 ± 1.05	(1.48± 0.41) × 10^5	8.19 ± 0.12	−29.51 ± 0.72	126.44 ± 0.73
HuHF in 50 mM Mops, 100 mM NaCl, pH 7.43 (Figure 4)	22.85 ± 0.81	(1.86 ± 0.65) × 10^5	8.77 ± 0.1	−30.07 ± 0.95	130.27 ± 0.97
HuHF in 100 mM Mops, 50 mM NaCl, pH 7.52 (Figure 5)	n_1 = 22.75 ± 0.92	K_1 = (1.47 ± 0.67) × 10^5	ΔH_1^0 = 5.67 ± 0.34	ΔG_1^0 = −29.49 ± 1.04	ΔS_1^0 = 117.92 ± 1.12
	n_2 = 73.90 ± 3.02	K_2 = (2.23 ± 0.27) × 10^3	ΔH_2^0 = 15.86 ± 0.91	ΔG_2^0 = −19.11 ±0.28	ΔS_2^0 = 117.28 ± 0.78
nucleation site variant A2 (E61A+E64A+E67A) in 100 mM Mes, 50 mM NaCl, pH 6.50 (Figure 6)	12.99 ± 0.31	(2.13± 0.68) × 10^6	8.99 ± 0.12	−36.12 ± 0.27	151.29 ± 0.35
3-fold channel variant S14 (D131I + E134F) in 50 mM Mops, 100 mM NaCl, pH 7.03 (Figure 7)	7.82 ± 0.51	(1.48 ± 0.64) × 10^5	7.45 ± 0.32	−29.51 ± 0.85	123.96 ± 0.91

[a] The reported thermodynamic quantities are apparent values and include the contributions to the overall equilibrium from ferritin and buffer species in different states of protonation. Standard errors from replicate determinations are indicated. Only values for the strong sites are reported (see footnote 3). [b] Calculated from $\Delta G° = -RT \ln K$. [c] Calculated from $\Delta S° = (\Delta H° - \Delta G°)/T$.

parameters obtained for the strong sites ($K \sim 10^5$ M^{-1}) but can influence the accuracy of values obtained for very weak binding ($K < 10^3$ M^{-1}). The data were collected automatically and analyzed using BindWorks 3.0 (Calorimetry Science Corporation, Provo, Utah). The mathematical models for one class of multiple independent binding sites or for two classes of independent multiple binding sites used for curve fitting in this study are described by Freire et al. (*26*). Typically the first data point of each titration is low due to loss of Fe^{2+} from the syringe needle to the cell prior to commencing the titration. Consequently, the first data point was usually not included in the fit. All ITC experiments were performed in 50 to 100 mM Mops or Mes buffer with 50−100 mM NaCl, pH 6.5−7.5. Conditions for the individual experiments are given in the figure captions. To investigate the effect of buffer on Fe^{2+} binding to ferritin, ITC measurements were also conducted with the protein in a phosphate buffer solution (18.75 mL of 0.2 M Na_2HPO_4 plus 31.25 mL of 0.2 M NaH_2PO_4) pH 6.6 at 25.00 °C (*28*). The thermodynamic parameters obtained were the same as those when Mes buffer pH 6.5 was employed.

The number of protons released per Fe^{2+} bound to the protein under anaerobic conditions was determined at 25 °C using a pH-stat apparatus (*17*). Typical conditions for these types of measurements were 0.5 to 1 μM protein in 100 mM NaCl and 0.3 mM Mes or Mops buffer, pH 6.5 or 7.5 (controlled by pH-stat), with increments of 12−48 Fe^{2+}/protein, added as freshly prepared ferrous sulfate solution in water at pH 3.5. To accurately measure the number of H^+ released upon Fe^{2+} binding to the protein anaerobically, a pH-stat proportional band setting of 0.2 was used. Background corrections for the free acid in the ferrous sulfate solutions were made in all calculations.

The time-dependent absorbance kinetic experiments of Fe^{2+} oxidation by O_2 in HuHF and its variants (Table 2) were performed on a Cary 50 Bio UV−visible spectrophotometer at 25 °C. The iron-free protein solution in buffer served as the blank. The specific Fe^{2+} oxidation activity per minute was calculated on a subunit basis from the initial rates of Fe^{2+} oxidation as measured by UV absorption spectroscopy at 305 nm using a molar absorptivity of 3000 M^{-1} cm^{-1} per iron (*17*).

Table 2: Specific Fe^{2+} Oxidation Activity of HuHF and Its Variants under Different Fe^{2+}/Protein Loading[a]

protein iron loading	specific Fe^{2+} oxidation activity (Fe/subunit·min)	relative activity at stated Fe^{2+} loading
wild-type HuHF		
48	44 ± 6 (N = 4)	100%
500	34 ± 3 (N = 3)	100%
1000	33 ± 4 (N = 4)	100%
1500	37 (N = 1)	100%
2000	36 (N = 1)	100%
nucleation site variant A2		
48	26 ± 3 (N = 3)	59%
500	28 ± 5 (N = 3)	82%
1000	23 (N = 1)	70%
3-fold channel variant S14		
48	1.7 ± 0.5 (N = 4)	4%
500	3.2 ± 0.2 (N = 2)	10%
1000	4.8 ± 0.5 (N = 2)	15%
1500	7.9 ± 0.3 (N = 2)	22%
2000	8.9 ± 0.3 (N = 2)	25%
ferroxidase site variant 222		
48	0.2 ± 0.01 (N = 2)	0.5%
500	0.4 ± 0.05 (N = 2)	1%

[a] Iron loadings are Fe/24mer protein shell. Conditions: 0.1 M Mops, 50 mM NaCl, pH 7.0. The protein concentrations were 1−2 μM for the 48 Fe^{2+}/shell experiments and 0.1 to 0.2 μM for the 500 to 2000 Fe^{2+}/shell experiments except for the nucleation site variant A2 where the protein concentration was 0.5 μM for both 500 and 1000 Fe^{2+}/shell. N is the number of determinations.

RESULTS

Fe^{2+} Binding to HuHF. ITC is the most quantitative means available for measuring the thermodynamic properties of any chemical reaction initiated by the addition of a binding component. When substances bind, heat is either generated or absorbed. Measurement of this heat allows the accurate determination of binding constants (K), reaction stoichiometries (n), enthalpies ($\Delta H°$), and entropies ($\Delta S°$), thus providing a complete thermodynamic profile of the molecular interaction in a single experiment. Figures 2A, 3A, and 4A show the injection heats for Fe^{2+} binding to HuHF at pH 6.51, 7.04, and 7.43 respectively, in dilute solution (~4 μM protein). The integrated heats (μJ) for each injection vs the molar ratio of Fe^{2+} to the apoprotein after subtraction of the

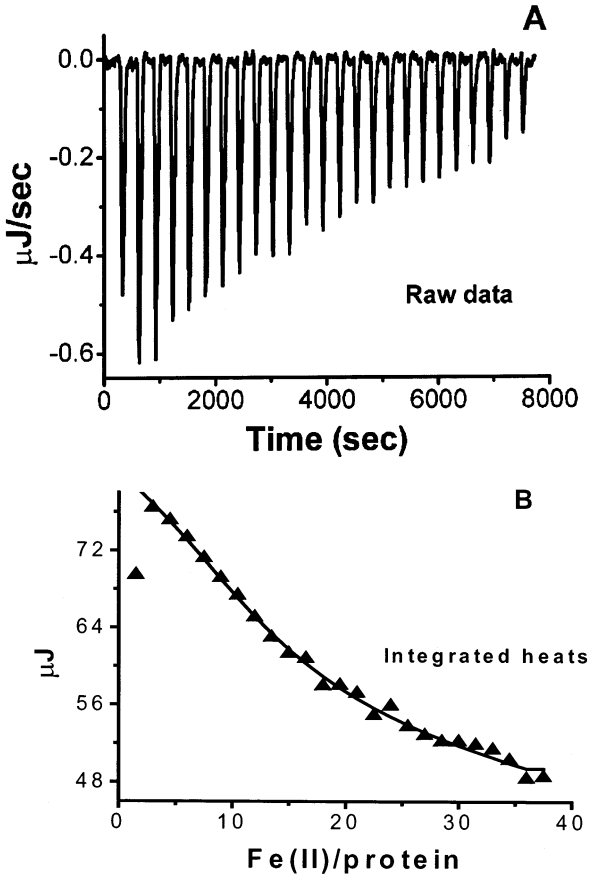

FIGURE 2: Calorimetric titration of HuHF with Fe^{2+} under anaerobic conditions. (A) Raw data. (B) Plot of the integrated heat versus the Fe^{2+}/protein molar ratio. Conditions: 4 μM HuHF titrated with 10 μL injections of 0.78 mM $FeSO_4$ in 50 mM Mes buffer, 100 mM NaCl, 1 mM $Na_2S_2O_4$, pH 6.51, and 25.00 °C.

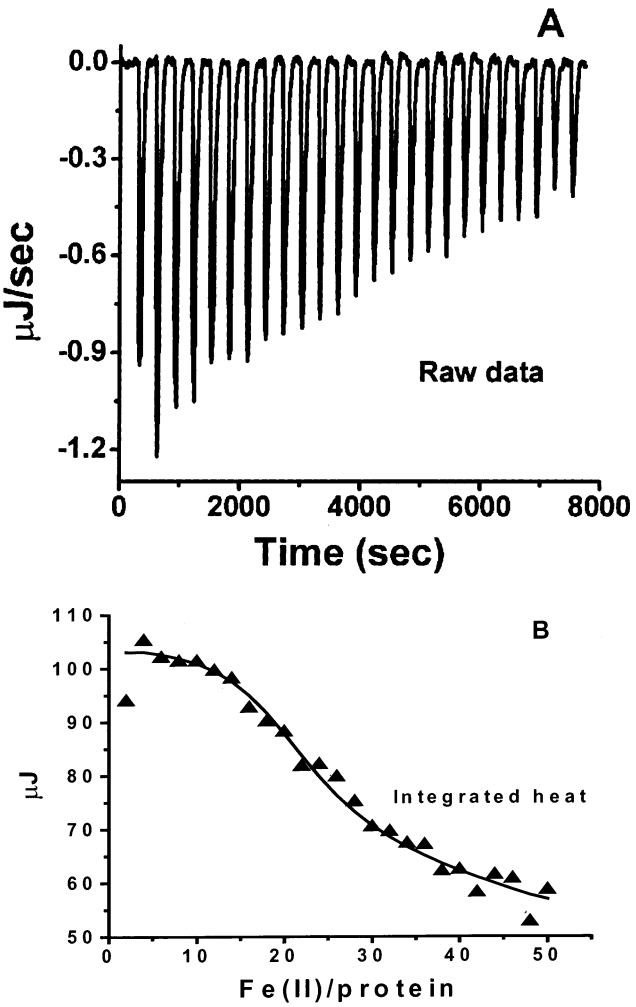

FIGURE 3: Calorimetric titration of HuHF with Fe^{2+} under anaerobic conditions. (A) Raw data. (B) Plot of the integrated heat versus the Fe^{2+}/protein molar ratio. Conditions: 4.33 μM HuHF titrated with 10 μL injections of 1.3 mM $FeSO_4$ in 50 mM Mops buffer, 100 mM NaCl, 1 mM $Na_2S_2O_4$, pH 7.04, and 25.00 °C.

heat of dilution of Fe^{2+} are illustrated in part B of each figure. Over the entire pH range, the negative peaks correspond to an endothermic reaction for Fe^{2+} binding.[2] The heats at the end of these titrations were in excess of the heat of dilution of Fe^{2+} (Figures 2B, 3B, and 4B), indicating additional weak binding on the protein. Accordingly, a model of two sets of independent binding sites, one strong and one weak, was used to curve fit all the data.[3] The derived parameters for the strong binding sites at pH 6.51, 7.04 and 7.43 are summarized in Table 1. Excellent fits are achieved. While titration of HuHF with Fe^{2+} in dilute solution at pH 6.51 results in a binding equilibrium with an inflection point at $n_1 \sim 12$ molar equivalents of Fe^{2+} per HuHF (Figure 2), ~24 molar equivalents are observed at pH 7.04 and 7.43 (Figures 3 and 4). The apparent binding constants increase slightly with increasing pH but the binding stoichiometry increases significantly from 12 to 24 (Table 1), implying a structural change in the protein between pH 6.5 and 7.0 allowing more Fe^{2+} to bind (see below).

The weak sites[3] observed at all pH values (6.51, 7.04 and 7.43) used in this work may reflect nonspecific binding to the protein or weak binding to functional sites that are only fractionally occupied under the conditions of the experiment. To better define the weak binding sites on the protein, a titration was carried out at pH 7.52 with 7-fold higher protein and iron concentrations. Figures 5A,B show the heats from Fe^{2+} binding to the protein at pH 7.52 and the curve fitting of the data, respectively, using a sum of two binding isotherm models, one involving two classes of independent binding sites, and the other, one class of independent binding sites.[4] From the thermodynamic parameters in Table 1, the first class ($n_1 \sim 24$, $K_1 \sim 1.5 \times 10^5$ M^{-1}) corresponds to Fe^{2+} binding to the same strong sites observed in dilute solution and the second class describes weak binding sites on the protein ($n_2 \sim 72$, $K_2 \sim 2.3 \times 10^3$ M^{-1}). The third class of sites represents very weak association of Fe^{2+} with the protein.[4]

Previous pH-stat measurements of Fe^{2+} binding to HoSF under anaerobic conditions showed little proton production

[2] The sign of the heat in the Figures is given relative to the CSC isothermal titration calorimeter. A negative measured heat corresponds to an endothermic Fe^{2+} binding reaction.

[3] Under the dilute solution conditions of these experiments where $K_2[L] \ll 1$, the individual thermodynamic parameters of the class of weak binding sites cannot be determined from the limiting form of the equation for two classes of binding sites (*26*). However, the product of the three parameters, $n_2K_2\Delta H_2$ was determined for HuHF to be (4.21 $\pm$ 1.31) $\times 10^6$ at pH 6.51, (1.33 $\pm$ 1.73) $\times 10^6$ at pH 7.04 and (1.44 $\pm$ 1.06) $\times 10^6$ at pH 7.43, for the nucleation site variant A2 (E61A + E64A + E67A) to be (5.87 $\pm$ 7.44) $\times 10^6$ at pH 6.51, for the 3-fold channel variant S14 (D131I + E134F) to be (1.00 $\pm$ 1.16) $\times 10^6$ at pH 7.03, and for the ferroxidase site variant 222 (E62K + H65G) to be (1.62 $\pm$ 1.03) $\times 10^6$ at pH 7.02 as calculated by the CSC curve fitting software.

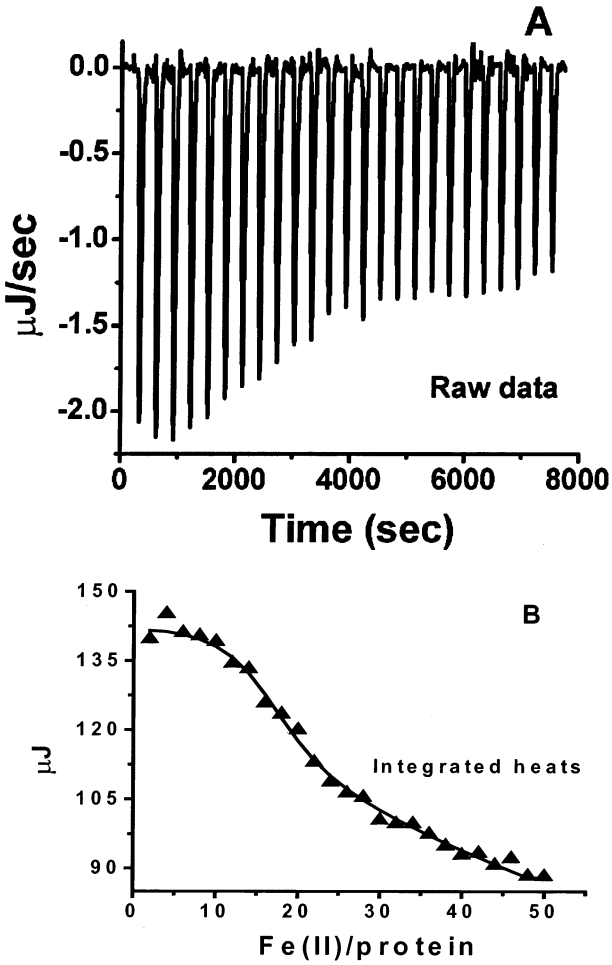

FIGURE 4: Calorimetric titration of HuHF with Fe^{2+} under anaerobic conditions. (A) Raw data. (B) Plot of the integrated heat versus the Fe^{2+}/protein molar ratio. Conditions: 4.33 μM HuHF titrated with 10 μL injections of 1.625 mM $FeSO_4$ in 50 mM Mops buffer, 100 mM NaCl, 1 mM $Na_2S_2O_4$, pH 7.43, and 25.00 °C.

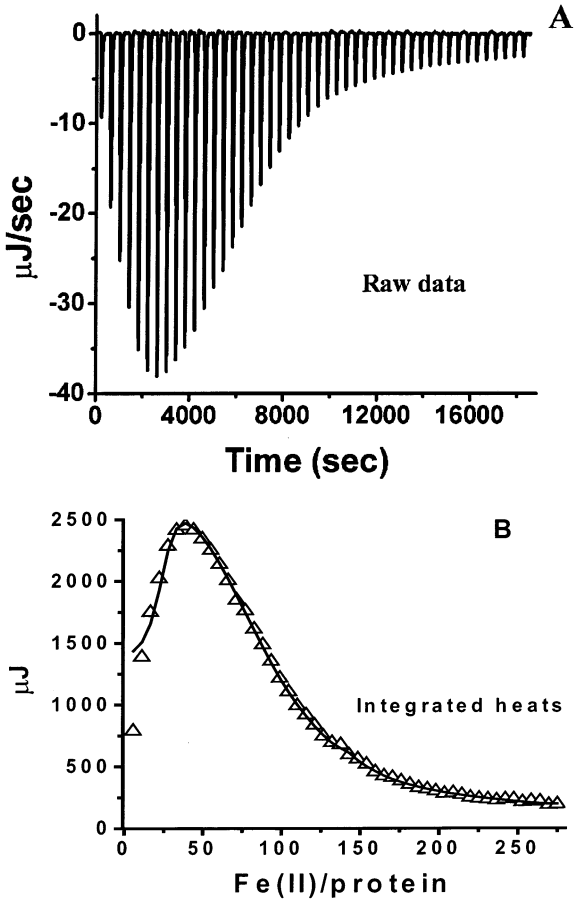

FIGURE 5: Calorimetric titration of HuHF with Fe^{2+} under anaerobic conditions. (A) Raw data. (B) Plot of the integrated heat versus the Fe^{2+}/protein molar ratio. Conditions: 28.2 mM HuHF titrated with 10 μL injections of 20.21 mM $FeSO_4$ in 100 mM Mops buffer, 50 mM NaCl, 1 mM $Na_2S_2O_4$, pH 7.52, and 25.00 °C. Figure 5 corresponds to two sequential titrations of 25 injections each for the same protein sample under the same conditions. The data were fit to the sum of two binding isotherms,[4] one involving two independent classes of binding sites (n_1 and n_2) and the other a single class of weak binding (n_3) commencing at an Fe^{2+}/HuHF ratio of 137/1.

(0.2 to 0.3 H^+/Fe^{2+}) upon Fe^{2+} binding prior to its oxidation (*17*). pH-stat experiments conducted here with HuHF also indicate fractional proton release upon Fe^{2+} binding to the apoprotein. At pH 6.5, 0.4 to 0.5 H^+ are produced per each of the 24 Fe^{2+} added to the protein. Since only 12 Fe^{2+} bind at pH 6.5, this result corresponds to $\sim$ 1 H^+ produced per Fe^{2+} bound. Similarly at pH 7.5 where 24 Fe^{2+} bind, a stoichiometry of 1 H^+/Fe^{2+} bound is obtained. Accordingly, we write eq 1 for ferrous binding to the apoprotein:[5]

$$Fe^{2+} + P^Z \rightleftarrows [P{-}Fe^{2+}]^{Z-1} + H^+ \qquad (1)$$

Equation 1 accounts in part for the increase in the amount of Fe^{2+} bound to the protein at higher pH. The "thermodynamic" concentration-based equilibrium constant K_{thermo} for the strong sites is related to the apparent value from ITC by $K_{thermo} = K_1[H^+] = 1.5 \times 10^{-2}$ at pH 7.0.

Fe^{2+} Binding to Ferroxidase Center Variant 222 (E62K + H65G) and Nucleation Site Variant A2 (E61A + E64A + E67A). The Fe^{2+} binding stoichiometry of $n_1 \sim 24$ observed with the wild-type protein implies the involvement of the 24 ferroxidase sites. To more firmly establish the locus of Fe^{2+} binding to ferritin, ITC experiments were carried out using ferroxidase and nucleation site variants 222 (E62K + H65G) and A2 (E61A + E64A + E67A), respectively. The double substitution of two ferroxidase site ligands, one bridging the two irons (Glu62) and the other directly binding

[4] Since a computer model of three classes of independent binding sites is not available, the first 25 data points of Figure 5 were fitted to a model of two classes of independent binding sites (n_1 and n_2), and the second 25 data points fitted independently to an another class of binding sites (n_3). The individual thermodynamic parameters of the class of weakest binding sites cannot be determined; however the product of the three parameters, $n_3K_3\Delta H_3$ was calculated to be $(1.14 \pm 0.61) \times 10^5$ from the CSC curve fitting software. The sharp transition between the 2nd and 3rd classes of binding sites shown in Figure 5B, the excellent curve fit and small errors in the values of the parameters obtained from each set of 25 data points (Table 1), and the agreement between the values of the n_1, K_1, and ΔH_1^0 obtained for concentrated (Figure 5) and dilute (Figure 4) protein solutions indicate that reliable parameters are obtained from this approach.

[5] Previously, it was assumed that no protons are produced during Fe^{2+} binding to HuHF based on the data for HoSF (*17*). The present result showing that 1 H^+ is produced from the binding of the first 24 Fe^{2+} to the apoprotein at pH 7.43 indicates that the source of at least one of the protons produced in eq 2 of ref 44 must come from Fe^{2+} binding to the protein. The second proton of eq 2 must arise from either the binding of the second Fe^{2+} to the ferroxidase sites or from the hydrolysis of the Fe^{3+} following oxidation.

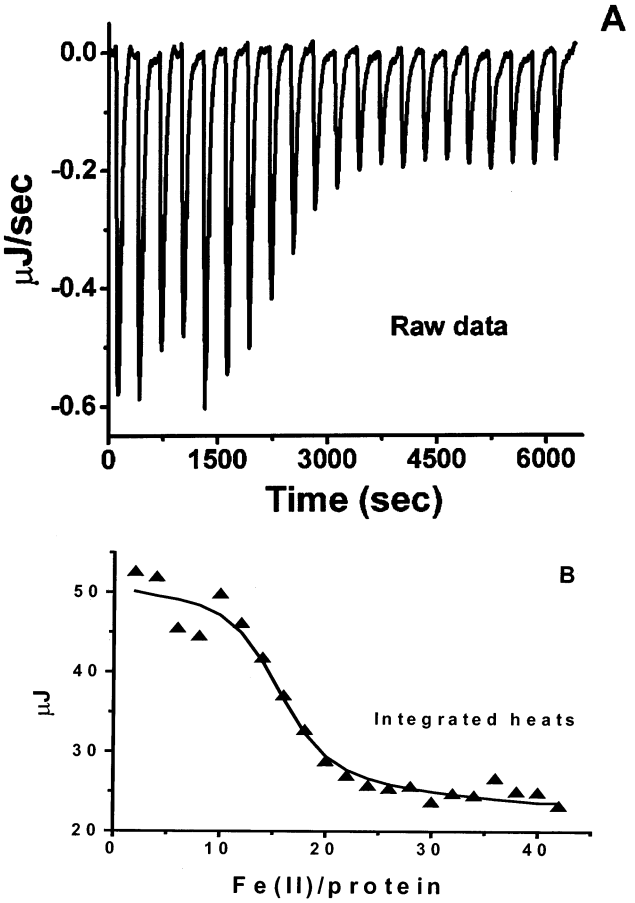

FIGURE 6: Calorimetric titration of the nucleation site variant A2 (E61A + E64A + E67A) with Fe^{2+} under anaerobic conditions. (A) Raw data. (B) Plot of the integrated heat versus the Fe^{2+}/protein molar ratio. Conditions: 3.6 μM A2 titrated with 10 μL injections of 0.92 mM $FeSO_4$ in 100 mM Mes buffer, 50 mM NaCl, 0.6 μM glucose oxidase (65 units), 0.2 mM glucose, 1 μL catalase (1300 units), pH 6.50, and 25.00 °C.

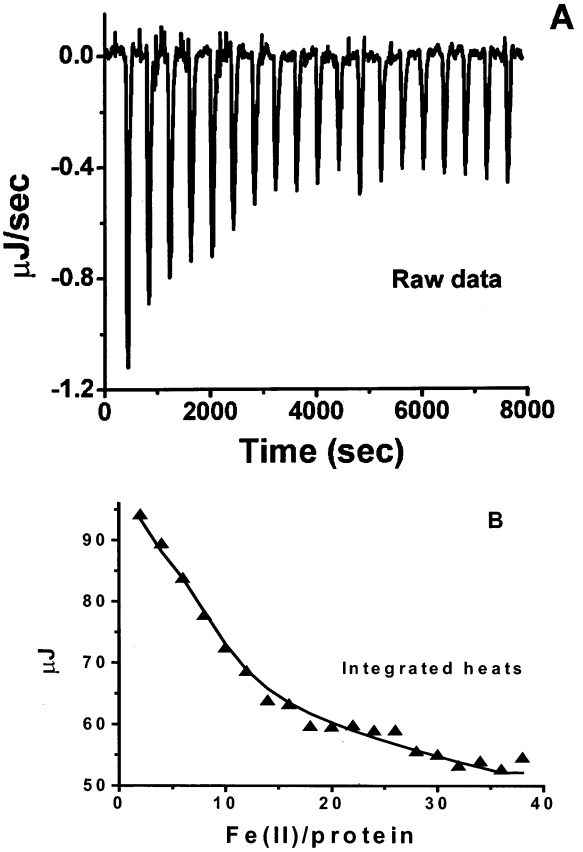

FIGURE 7: Calorimetric titration of the 3-fold channel variant S14 (D131 + E134F) with Fe^{2+} under anaerobic conditions. (A) Raw data. (B) Plot of the integrated heat versus the Fe^{2+}/protein molar ratio. Conditions: 5.0 μM S14 titrated with 10 μL injections of 1.3 mM $FeSO_4$ in 50 mM Mops buffer, 100 mM NaCl, 1 mM $Na_2S_2O_4$, pH 7.03, and 25.00 °C.

to one of them (His65) as in Figure 1, completely eliminated the strong binding of Fe^{2+} at pH 7.0 observed with the wild-type protein (Figure 3) while weak binding was retained,[3] implying that iron binding in dilute solution primarily occurs at the ferroxidase center within the H-chain subunit. On the other hand, the nucleation site variant A2 (E61A + E64A + E67A) binds the same amount of Fe^{2+} as the wild-type protein at pH 6.5 (Figure 6, Table 1), indicating that nucleation site residues, Glu61, Glu64, and Glu67 are not critical to Fe^{2+} binding.

Fe^{2+}Binding to the 3-Fold Channel Variant S14 (D131I + E134F). ITC binding experiments were also performed on the recombinant 3-fold channel variant S14 (D131I + E134F). Figure 7 shows the raw ITC data for a titration of S14 with Fe^{2+} at pH 7.03 and the integrated heats for each injection after subtraction of the control injection. In the S14 variant, alteration of the channel Asp131 and Glu134 ligands did not completely eliminate the binding of iron but had a pronounced effect on the binding stoichiometry, reducing it to one-third of that for the wild-type protein. An endothermic reaction is seen with a binding stoichiometry of ~8 molar equivalents per protein at pH 7.03 (Table 1). An excellent fit of the data (Figure 7B) is achieved for a model with two sets of independent binding sites (Table 1).[3]

Specific Fe^{2+} Oxidation Activity of HuHF and Its Variants. The specific Fe^{2+} oxidation activity per subunit measured from the initial rates in the wild-type protein HuHF, the nucleation site variant A2, the 3-fold channel variant S14 and the ferroxidase center variant 222 were determined at different Fe^{2+}/protein loadings (Table 2). The results in Table 2 indicate that the nucleation site variant A2 is nearly as active as the wild type protein. In contrast, the specific activity of the 3-fold channel variant S14 is markedly lower in accord with the ITC data showing the critical importance of intact 3-fold channels for full Fe^{2+} binding at the ferroxidase center. Expectedly, ferroxidase site variant 222 shows little activity.

DISCUSSION

The goal of the present investigation was to identify the Fe^{2+} binding sites on the protein prior to its oxidation and to characterize this binding thermodynamically. Previous kinetic and binding studies have shown that, in the presence of molecular oxygen, two Fe^{2+} ions appear to be oxidized cooperatively, or nearly so, at each of the 24 ferroxidase centers of HuHF (*17*, *29*). A transient blue intermediate (λ_{max} = 650 nm) has been ascribed to a μ-1,2-peroxodiFe(III) intermediate formed at the ferroxidase site (*30*), an assignment confirmed recently by Mössbauer spectroscopy measurements (*31*). Stopped-flow absorption, freeze-quench Mössbauer and resonance Raman spectroscopic investigations have also shown that a peroxodiferric intermediate is formed during the oxidation of Fe^{2+} in recombinant frog M

apoferritin, BfMF (*32*, *33*). Taken together, these results imply that Fe^{2+} binds pairwise at the ferroxidase center of ferritins. However, the present data demonstrate that, under dilute solution conditions comparable to those in previous kinetic studies but in the absence of molecular oxygen, only 24 Fe^{2+} strongly bind to the protein, one per ferroxidase center. The binding of the second Fe^{2+} evidently does not appreciably occur unless O_2 is present. This result suggests an important role of molecular oxygen and indicates that a two step process of Fe^{2+} binding/oxidation likely occurs. A stopped-flow investigation of Fe^{2+} binding and oxidation in EcFtnA and HuHF is consistent with this observation, showing a preferred order of binding of Fe^{2+} to the ferroxidase sites (*29*). From the kinetic data, it was concluded that Fe^{2+} binds first at site A and then at site B, and that dioxygen binds to site B but not to site A (Figure 1). In the absence of molecular oxygen, the binding of the 24 Fe^{2+} seen with HuHF by ITC, most likely occurs at site A which contains mixed oxygen and nitrogen ligands (Figure 1) that would favor Fe^{2+} binding, and that Fe^{2+} binding and oxidation at site B requires the presence of O_2. The possibility that a small fraction of ferroxidase centers are doubly occupied by Fe^{2+} and are the catalytically active species is not precluded by the data, however. The heats observed at the end of the titration curves in Figures 2B, 3B, and 4B for dilute protein solutions are due to weak binding of Fe^{2+} to the protein (Results).

Experiments undertaken at high protein and iron concentrations (Figure 5) more clearly indicate the presence of weak binding sites with a stoichiometry of $n_2 \sim 72$ Fe^{2+}/shell. We suggest that the 24 Fe^{2+}/shell expected from Fe^{2+} binding to the B sites are included in this second class of sites and that the remaining 48 Fe^{2+} of the $n_2 \sim 72$ total are bound elsewhere. The binding constants of the two groups of 24 and 48 Fe^{2+} are too close to be resolved by the data, but they are ~66-fold less than that of the strong n_1 sites (Table 1). The weakest class of binding sites, n_3, may represent nonspecific binding to the protein. The reduction in stoichiometry for strong binding from 24 Fe^{2+}/shell at pH 7.0 to 12 Fe^{2+}/shell at pH 6.5 (Table 1) in dilute solution is consistent with Fe^{2+} binding to the histidine containing site A, as histidine pK_a's are typically in this pH range. The pH dependence of the initial rate of iron oxidation in HuHF has been attributed to the deprotonation of the histidine residue at the ferroxidase center, the maximum rate being obtained at pH 7.0 (*34*) where Fe^{2+} binding is maximized at 24 Fe^{2+}/protein (Table 1).

Alteration in the ferroxidase center ligands Glu62 and His65 in variant 222 totally eliminates strong Fe^{2+} binding to the protein (data not shown), a result confirming the importance of one or both of these residues in the ferroxidase activity (Table 2). Consistent with this observation, previously reported UV and Mössbauer spectroscopy studies on the ferroxidase center variant 222 (E62K + H65G) have shown reduced Fe^{2+} oxidation, requiring more than 2.5 h for completion (*16*, *24*, *35*). In contrast, nucleation site variant A2 (E61A + E64A + E67A) exhibits very similar Fe^{2+} binding behavior to HuHF (Figure 6) indicating that the putative nucleation site ligands (Glu61, Glu64, and Glu67) do not play an important role in Fe^{2+} binding to ferritin even though Glu61 is a shared ligand between the ferroxidase and nucleation sites. This finding is in agreement with previous kinetic data showing that the nucleation site variant A2 (E61A + E64A + E67A) exhibits only a slight decrease in the rate of Fe^{2+} oxidation under conditions of low iron loading (<50 Fe/shell) to the apoprotein (*34*) (also Table 2).

The data in Figure 7 and Table 1 show that the 3-fold channel variant S14 (D131I + E134F) strongly binds only about one-third as much Fe^{2+} as HuHF. This value is comparable with the relative rates of iron oxidation at high Fe^{2+}/protein ratios of 1000−2000 reported for variants bearing substitutions at the 3-fold channel as compared to HuHF (*10*, *11*, *13*, Table 2). The ITC result in Figure 7 clearly shows the importance of the 3-fold channels as pathways for Fe^{2+} to the catalytic oxidation centers, a finding consistent with the 3-fold channels being the primary route by which Fe^{2+} traverses the protein shell to the ferroxidase centers where it is oxidized, ultimately forming the mineral core (*10*, *12*−*14*, *36*). Recent studies employing spin probes and size exclusion chromatography have provided further evidence that the 3-fold channels are the principal pathways for molecular diffusion into ferritin (*37*). Moreover, substitutions of conserved amino acids at the 3-fold channels of the amphibian H-chain ferritin have important effects on the rates of iron entry and exit through the protein coat (*38*−*40*). Alteration of the 3-fold channel residues (Asp131 and Glu134) in HuHF reduces the ability of the subunits to assemble into a stable compact structure, inducing a conformational change in the protein (*11*). DSC shows greatly reduced thermal stability of the channel variant S14 compared to HuHF, an indication that intersubunit contacts along the 3-fold axes are important for protein shell assembly (*41*). The results presented here suggest that in the case of an altered 3-fold channel, about one-third of the ferritin shells appears to remain permeable to iron, enabling it to ultimately reach the ferroxidase centers. The enthalpies and equilibrium constants of HuHF and variant S14 are essentially identical (Table 1), the only difference being that the variant binds only ~8 Fe^{2+}/shell at pH 7.0 compared to 24 Fe^{2+}/shell for the wild-type protein.

The specific activity of the 3-fold channel variant S14 lacking Asp and Glu residues is low relative to HuHF but increases with increasing iron concentration in the bulk solution, approaching a limiting value of about 25% that of HuHF (Table 2). Such behavior is consistent with molecular diffusion across the protein shell being the limiting factor in the observed rate of Fe^{2+} oxidation at the lower Fe^{2+}/protein ratios. The data suggest that the carboxylate groups of the 3-fold channels are essential for rapid iron transport across the protein shell in accord with recent molecular diffusion studies of ferritin (*37*). Other experiments have suggested that the 3-fold channels may function as dynamic apertures for iron entry and exit (*13*, *38*).

Some of the additional weak Fe^{2+} binding sites on the protein of the $n_2 \sim 48$ and of the n_3 classes of binding sites seen in Figure 5 under conditions of high concentration protein and iron solutions[4] (Table 1) are perhaps located in or near the outer opening of the eight 3-fold channels. This interpretation is consistent with earlier reports showing that residues exposed on the 3-fold channels play an active role in the mechanism of iron incorporation into ferritin (*13*). More recently, a study employing site-directed mutagenesis

and EPR spectroscopy revealed the presence of vanadium (VO^{2+}) binding sites involving His118 located near the outer opening of the 3-fold channel, a ligand also suggested to be a binding site for Fe^{2+} (*42*).

The large positive entropy of Fe^{2+} binding to the ferroxidase center over the pH range of 6.5 to 7.5 (average $\Delta S^0 \sim$ 130 J/mol·K) and small endothermic $\Delta H°$ (average $\Delta H° \sim$ 8.40 kJ/mol) indicate that Fe^{2+} binding to the A-sites of HuHF is an entropy driven process (Table 1). The most likely contributions to such a positive entropy $\Delta S°$ observed are the changes in the hydration of the protein and of the Fe^{2+} ion upon binding to the protein (*43*).

In summary, this study indicates that the 3-fold channels are the most important pathways for iron entry into ferritin, establishes that the principal site of Fe^{2+} binding is at the ferroxidase center and shows the critical role of intact ligands at this center for Fe^{2+} binding. Furthermore, the ITC data indicate that the first step in the mechanism of iron deposition in ferritin probably corresponds to the binding of a single Fe^{2+} initially at the ferroxidase center (most likely site A). The binding and oxidation of the second Fe^{2+} at site B of the di-iron center may be facilitated by O_2 binding and/or oxidation of the first Fe^{2+} to yield the spectroscopically observed μ-peroxo- and μ-oxo-diferric species (*17*, *30*, *31*). The data also show that there are multiple weak binding sites on the protein, the origin of which remains to be definitively established.

REFERENCES

1. Arosio, P., Adelman, T. G., and Drysdale, J. W. (1978) *J. Biol. Chem.* 253, 4451−4458.
2. Lawson, D. M., Artymiuk, P. J., Yewdall, S. J., Smith, J. M. A., Livingstone, J. C., Treffry, A., Luzzago, A., Levi, S., Arosio, P., Cesareni, G., Thomas, C. D., Shaw, W. V., and Harrison, P. M. (1991) *Nature 349*, 541−544.
3. Harrison, P. M., and Arosio, P. (1996) *Biochim. Biophys. Acta 1275*, 161−203.
4. Michaux, M. A., Dautant, A., Gallois, B., Granier, T., D'Estaintot, B. L., and Precigoux, G. (1996) *Proteins 24*, 314−321.
5. Harrison, P. M., Hempstead, P. D., Artymiuk, P. J., and Andrews, S. C. (1998), in *Metal Ions in Biological Systems* (Sigel, A., and Sigel, H., Eds.) Vol. 35, pp 435−477, Marcel Dekker, Inc., New York.
6. Harrison, P. M., Andrews, S. C., Artymiuk, P. J., Ford, G. C., Guest, J. R., Hirzmann, J., Lawson, D. M., Livingstone, J. C., Smith, J. M. A., Treffry, A., and Yewdall, S. J. (1991) *Adv. Inorg. Chem. 36*, 449−486.
7. Hempstead, P. D., Hudson, A. J., Artymiuk, P. J., Andrews, S. C., Banfield, M. J., Guest, J. R., and Harrison, P. M. (1994) *FEBS Lett. 350*, 258−262.
8. Wade, V. J., Levi, S., Arosio, P., Treffry, A., Harrison, P. M., and Mann, S. (1991) *J. Mol. Biol. 221*, 1443−1452.
9. Treffry, A., Harrison, P. M., Luzzago, A., and Cesareni, G. (1989) *FEBS Lett. 247*, 268−272.
10. Treffry, A., Bauminger, E. R., Hechel, D., Hodson, N. W., Nowik, I., Yewdall, S. J., and Harrison, P. M. (1993) *Biochem. J. 296*, 721−728.
11. Levi, S., Luzzago, A., Franceschinelli, F., Santambrogio, P., Cesareni, G., and Arosio, P. (1989) *Biochem. J. 264*, 381−388.
12. Desideri, A., Stefanini, S., Polizio, F., Petruzelli, R., and Chiancone, E. (1991) *FEBS Lett. 287*, 10−14.
13. Levi, S., Santambrogio, P., Corsi, B., Cozzi, A., and Arosio, P. (1996) *Biochem. J. 317*, 467−473.
14. Ford, G. C., Harrison, P. M., Rice, D. W., Smith, J. M. A., Treffry, A., White J. L., and Yariv, J. (1984) *Philos. Trans. R. Soc. London B 304*, 551−565.
15. Xu, B., and Chasteen, N. D. (1991) *J. Biol. Chem. 266*, 19965−19970.
16. Treffry, A., Hirzmann, J., Yewdall, S. J., and Harrison, P. M. (1992) *FEBS Lett. 302*, 108−112.
17. Yang, X., Barrett, Y. C., Arosio, P., and Chasteen, N. D. (1998) *Biochemistry 37*, 9743−9750.
18. Waldo, G. S., and Theil, E. C. (1996) in *Comprehensive Supramolecular Chemistry* (Suslick, K. S., Ed.) Vol. 5, pp 65−89.
19. Chasteen, N. D. (1998) in *Metal Ions in Biological Systems* (Sigel, A., and Sigel, H., Eds.) Vol. 35, pp 479−514, Marcel Dekker, Inc., New York.
20. Chasteen, N. D., and Harrison, P. M. (1999) *J. Struct. Biol. 126*, 182−194.
21. Hilty, S., Webb, B., Frankel R. B., and Watt, G. D. (1994) *J. Inorg. Biochem. 56*, 173−185.
22. Studier, F. W., and Moffatt, B. A. (1986) *J. Mol. Biol. 189*, 113−130.
23. Levi, S., Luzzago, A., Cesareni, G., Cozzi, A., Franceschinelli, F., Albertini, A., and Arosio, P. (1988) *J. Biol. Chem. 263*, 18086−18092.
24. Bauminger, E. R., Harrison, P. M., Hechel, D., Nowik, I., and Treffry, A. (1991) *Biochim. Biophys. Acta 1118*, 48−58.
25. Zhao, G., Bou-Abdallah, F., Yang, X., Arosio, P., and Chasteen, N. D. (2001) *Biochemistry 40*, 10832−10838.
26. Freire, E., Mayorga, O. L., and Straume, M. (1990) *Anal. Chem. 62*, 950A−959A.
27. Briggner, L. E., and Wadsö, I. (1991) *J. Biochem. Biophys. Methods 22*, 101−118.
28. Dawson, R. M. C., Elliott, D. C., Elliott, W. H., and Jones, K. M. (1969) in *Data for Biochemical Research* 2nd. ed. Oxford University Press: New York.
29. Treffry, A., Zhao, Z., Quail, M. A., Guest, J. R., and Harrison, P. M. (1997) *Biochemistry 36*, 432−441.
30. Zhao, Z., Treffry, A., Quail, M. A., Guest, J. R., and Harrison, P. M. (1997) *J. Chem. Soc., Dalton Trans.* 3977−3978.
31. Bou-Abdallah, F., Papaefthymiou, G. C., Scheswohl, D. M., Stanga, S. D., Arosio, P., and Chasteen, N. D. (2002) *Biochem. J. 364*, 57−63.
32. Pereira, A. S., Small, W., Krebs, C., Tavares, P., Edmondson, D. E., Theil, E. C., and Huynh, B. H. (1998) *Biochemistry 37*, 9871−9876.
33. Moënne-Loccoz, P., Krebs, C., Herlihy, K., Edmondson, D. E., Theil, E. C., Huynh, B. H., and Loehr, T. M. (1999) *Biochemistry 38*, 5290−5295.
34. Sun, S., Arosio, P., Levi, S., and Chasteen, N. D. (1993) *Biochemistry 32*, 9362−9369.
35. Bauminger, E. R., Harrison, P. M., Hechel, D., Nowik, I., and Treffry, A. (1991) *Proc. R. Soc. London B 244*, 211−217.
36. Harrison, P. M., Treffry, A., and Lilley, T. H. (1986) *J. Inorg. Biochem. 27*, 287−293.
37. Yang, X., Arosio, P., and Chasteen, N. D. (2000) *Biophys. J. 78*, 2049−2059.
38. Takagi, H., Shi, D., Ha, Y., Allewell, N. M., and Theil, E. C. (1998) *J. Biol. Chem. 273*, 18685−18688.
39. Jin, W., Takagi, H., Pancorbo, B., and Theil, E. C. (2001) *Biochemistry 40*, 7525−7532.
40. Theil, E. C., Takagi, H., Small, G. W., He, L., Tipton, A. R., and Danger, D. (2000) *Inorg. Chim. Acta 297*, 242−251.
41. Budzinski, L. M. (2000) M. S. Thesis, University of New Hampshire, Durham, 129 pp.
42. Grady, J. K., Shao, J., Arosio, P., Santambrogio, P., and Chasteen, N. D. (2000) *J. Inorg. Biochem. 80*, 107−113.
43. Sundstrom, M., Hallen, D., Svensson, A., Schad, E., Dohlsten, M., and Abrahmsen, L. (1996) *J. Biol. Chem. 271*, 32212−32216.
44. Yang, X., Le Brun N. E., Thomson, A. J., Moore, G. R., and Chasteen, N. D. (2000) *Biochemistry 39*, 4915−4923.

BI020215G